

Original Research

Preliminary Study of Methyl Orange Removal Using a Persulfate-Based Advanced Oxidation Process with Indonesian Palm Kernel Shell-Based Activated Carbon as an Activator: Experiment and Sorption-Oxidation Kinetic Analyses

Setiyono^{1,2}, Heru Susanto³, Sudarno⁴, Muhammad Abdul Kholiq⁵, Veny Luvita¹, Rudi Nugroho¹, Nusa Idaman Said¹, Ahmad Shoiful¹, Nicolaus Nezha Nunez Mahasti¹, Nur Muhamad Fuad¹, Sandia Primeia¹, Ikkal¹, Arifudin¹, Taty Hernaningsih¹, Wahyu Widayat¹, Yosep Widi Nugraha¹, Fajar Eko Priyanto¹, Joko Waluyo⁶, Reza Yuridian Purwoko⁷, Ardie Septian^{1*}

¹Research Center for Environmental and Clean Technology, National Research and Innovation Agency (BRIN), Building 720, K.S.T. B.J Habibie, Serpong, South Tangerang 15314, Indonesia

²Graduate School of Environmental Studies, Diponegoro University, Jl. Prof. Soedarto SH Tembalang, Semarang 50275, Indonesia

³Chemical Engineering Diponegoro University, Jl. Prof. Soedarto SH Tembalang, Semarang 50275, Indonesia

⁴Environment Engineering Diponegoro University, Jl. Prof. Soedarto SH Tembalang, Semarang 50275, Indonesia

⁵Directorate for Environment, Maritime, Natural Resources, and Nuclear Policy, National Research and Innovation Agency (BRIN), Gedung B.J. Habibie, Jl. M.H. Thamrin No. 8, Jakarta, Indonesia

⁶Program Studi Teknik Kimia, Sebelas Maret University, Jl. Ir. Sutami No. 36, Surakarta, Indonesia

⁷Research Center for PreClinical and Clinical Medicine, National Research and Innovation Agency (Badan Riset dan Inovasi Nasional, BRIN), Jl. Raya Bogor KM. 46, Cibinong 16911, Indonesia

Received: 5 October 2024

Accepted: 16 December 2024

Abstract

Two types of activated carbon (AC), namely Indonesian palm kernel shell-based AC (ZnCl₂-AC) and commercial AC, were introduced to activate persulfate (PS) for catalytic degradation of methyl orange (MO) in water. This is the first attempt to apply the coupled sorption-oxidation kinetic model to the kinetic data of MO removal in the PS/AC system. The PS activated by AC removed more MO than the AC-only or PS activated by Fe²⁺. In the PS/AC system, to get maximum MO removal (100%), the use of commercial AC needed higher AC and PS dosages ([AC] = 185 mg L⁻¹, and [PS] = 346 mg L⁻¹) than the use of ZnCl₂-AC ([AC] = 770 mg L⁻¹, and [PS] = 1728 mg L⁻¹). The MO removal in the PS/AC

system fitted with the coupled sorption–oxidation kinetic model. Compared to the AC-only system, the PS/AC system enhanced the oxidation mechanism but depressed the sorption mechanism. The $O_2^{\cdot-}$ played a dominant role in the oxidation mechanism. The MO was degraded through demethylation, carboxylation, ring opening, azo bond breakage, asymmetric cleavage, and aromatic ring removal.

Keywords: activated carbon, methyl orange, oxidation, persulfate, textile wastewater

Introduction

The textile industry is a long-established industry in Indonesia. The textile industry has existed since the seventh century and originated in central Java. Indonesian textiles are one of the export commodities that can potentially increase the country's economy. However, the activities of textile industries result in wastewater. Textile wastewater has toxic and dangerous chemical contents [1]. Apart from the toxicity concerns, the textile industries generate a huge amount of this waste, around 50 to 240 m³ ton⁻¹ of textile products [2]. The characteristics of textile wastewater vary due to the type and process of textile production, as well as the raw materials used [3, 4].

Based on the survey studies, the textile industries consume 164 (±81.8) L of water kg⁻¹ of pre-dyeing material and 136 (±70.6) L of water kg⁻¹ of dyeing final products [5]. Dyes are the largest source of textile wastewater. Dyes are also usually used in other industries, including cosmetics, leather, pharmaceuticals, printing, paper, plastic, and food. Synthetic organic dyes have become a major ecological contaminant in polluted water because they have characteristics of low biodegradation, chemical stability, toxic and carcinogenic properties, and high aromaticity [6, 7]. During the dyeing process, a large amount of dye material (around 10-15%) is lost and discharged into the water bodies [6, 8].

The dye molecule combines unsaturated organic substances, chromophores (color carriers), and auxochromes (color-fiber binders). Chromophores are color-giving substances derived from chemical radicals, such as nitroso groups, nitro groups, azo groups, ethylene groups, carbonyl groups, carbon-nitrogen groups, and sulfur groups. More broadly, dyestuffs comprise unsaturated hydrocarbons, chromogens, auxochromes, and additives (migration, leveling, wetting agents, etc.). These unsaturated organic chemicals are primarily derived from aromatic compounds and their derivatives (toluene, benzene, xylene, anthracene, naphthalene), phenols and their derivatives (phenol, orth/meta/para cresol), and nitrogen-containing compounds (pyridine, kinolin, and corbazolum). The dyes used in the textile dyeing process are auxosomal groups made up of two groups, namely cations (-NH₂, NHR, -NR₂), such as NR₂ Cl, and anion groups (-SO₃H, -OH, -COOH). Various colors can be obtained by combining these

chemical radicals with other chemical compounds [1, 9, 10].

One of the dyes widely used in the textile coloring process is Methyl Orange (MO). MO, with a chemical formula of C₁₄H₁₄N₃NaO₃S, is an anionic azo-type dye widely utilized in the textile, papermaking, leather tanning, and food manufacturing industries. It has the potential to pollute the environment and enter the food chain due to its water-soluble characteristics [7, 11]. Living organisms are affected by textile wastewater. Therefore, it needs to be treated before being released into the water body.

Textile industrial wastewater has been widely treated using conventional techniques, such as chemical, physical, and biological processes, and advanced processes, including photocatalysis, bio-adsorbents, and advanced oxidation processes (AOPs) [12-14]. However, the massive production of photo-catalysts and the energy consumption of nanobubble generators and plasma at an industrial scale for producing reactive oxygen species (ROS) are still not economically feasible. In terms of low-cost implementation, persulfate (PS) can be used as an oxidant in AOPs due to its affordable price for industrial applications. Our previous studies reported that the PS was effectively activated by Fe²⁺ [15], colloidal activated carbon [16], and electrochemical oxidation [17] for acenaphthene, phenol, and 2-methylnaphthalene complete removals, respectively. The benefit of these activation studies is that the AOPs system showed outstanding removal efficiencies up to 3-4 cycles, where non-radical species (singlet oxygen, ¹O₂) [18] and radical species (SO₄^{·-}, ·OH, and O₂^{·-}) of ROS played essential roles in the degradation mechanisms.

Persulfate (PS) is widely used to degrade organic contaminants in wastewater. The PS contains anion S₂O₈²⁻ which can be activated by heat, Fe(II), colloidal activated carbon, and electrochemical oxidation to generate hydroxyl radical (·OH), sulfate radical (SO₄^{·-}), and superoxide radical (O₂^{·-}) [15, 16, 19, 20]. These radical species are effective in degrading phenol and polycyclic aromatic hydrocarbons (PAHs), such as 2-methylnaphthalene and acenaphthene, up to 75.2-100% [15, 17]. Among the activators, activated carbon has many advantages, including relatively cheap cost, substantial surface area, elevated adsorption capacity, and reactivation ability [17]. The utilization of activated carbon (AC) to activate PS for removing some pollutants (pharmaceuticals, perfluorooctanoic

acid (PFOA), and 1,4-dioxane) has been conducted by previous studies [20, 21]. Based on the information above, the utilization of activated carbon (AC) to activate PS, which is then applied to remove MO in textile wastewater, has not been investigated.

Activated carbon comes from carbonaceous raw materials, namely coal, wood, coconut, and biowaste, through two main processes: carbonization and activation. Palm kernel shell (PKS), a solid waste generated during palm oil manufacturing, has a high potential for activated carbon production due to its abundance. In a palm oil mill, approximately 65 kg PKS is generated from every ton of fresh fruit bunches and palm oil. In 2019, 17 million tons (Mt) of PKS were produced from the total production of fresh fruit bunches (FFB) of 256 Mt [22].

Using Indonesian palm kernel shell-based activated carbon as an activator for PS in treating MO pollutants is novel and attractive. In this method, two problems can be solved simultaneously: palm kernel shell waste and MO pollutants in wastewater. On the other hand, the enormous production of PKS waste provides a sustainable availability of the activated carbon raw material. Thus, the current research intends to study the catalytic degradation of MO in wastewater using PS with the Indonesian palm kernel shell-based activated carbon as an activator. Based on our best literature review, this research is the first attempt to investigate the utilization of PS activated by AC to remove MO. The Indonesian palm kernel shell-based AC was prepared through pyrolysis using ZnCl_2 as a modifier agent (symbolized as AC- ZnCl_2). The ZnCl_2 was used to investigate the influence of modification on the AC's performance as a catalyst. The performance of the AC- ZnCl_2 and the commercial AC in removing MO was also compared. The optimum ratio of AC and PS was determined. The existence of radical species in the reaction was identified using electron spin resonance (ESR). The resulting byproducts of MO degradation were also analyzed. Finally, the pathway of MO degradation was proposed and discussed.

Experimental

Materials

Aqueous solutions of MO and stock solutions of PS (100 mM) and Fe^{2+} (100 mM) were made by dissolving MO, sodium persulfate ($\text{Na}_2\text{S}_2\text{O}_8$; $\geq 99\%$, ACS Reagent, Sigma-Aldrich, USA), and ferrous sulfate heptahydrate ($\text{FeSO}_4 \cdot 7\text{H}_2\text{O}$; 98–100%, Duksan Pure Chemicals Co., Ltd., Korea) in water, respectively. Zinc chloride (ZnCl_2 ; 98%, Extra Pure, Duksan Pure Chemicals Co., Ltd., Korea) was used as an agent for activated carbon modification. The (FFA) commercial AC was purchased from a local company in Indonesia. The synthesized AC was produced from palm kernel shells, which were obtained from a company in Indonesia.

Synthesis of Activated Carbon from Palm Kernel Shell

The palm kernel shells were crushed to 40-60 mesh size, then washed and dried before carbon activation. The dried palm kernel shell was then placed in the pyrolysis reactor with up to 10 g, and 1 g ZnCl_2 was added. The activation process was carried out for 30 minutes at temperatures of 700°C using N_2 as a carrier at a flow rate of 200 mL/min [23, 24]. Further, in this study, the resulting Indonesian palm kernel shell-based AC was named ZnCl_2 -AC. HACH COD reagents (Low Range (2-150 mg L^{-1}) and High Range (20-1500 mg L^{-1}), Hach Company, USA) were utilized to measure the chemical oxygen demand (COD). Formic acid (liquid chromatography grade, 99.9%, Merck, USA) and acetonitrile (liquid chromatography grade, LiChrosolv®, Germany) were utilized as mobile phases in HPLC-MS analysis. All ACS-grade chemicals were utilized without further purification and dissolved in distilled and de-ionized (DDI) water (MilliporeSigma™ Synergy™ Ultrapure Water Purification System, Thermo Fisher Scientific, USA).

Physico-Chemical Properties of ACs

The BET surface areas (A_{BET}) were observed from the N_2 adsorption-desorption data and fitted to the Brunauer-Emmett-Teller (BET) model (Quantachrome, Autosorb-iQ & Quadrasorb Si, USA). The surface morphology was observed using field emission-scanning electron microscopy (FE-SEM, JEOL JSM-7001F, National Research and Innovation Agency of Indonesia). The commercial AC and ZnCl_2 -AC particle size distribution were measured using a dynamic light scattering (DLS, Malvern Panalytical Ltd., Mastersizer 3000, UK).

Experimental Design and Procedure

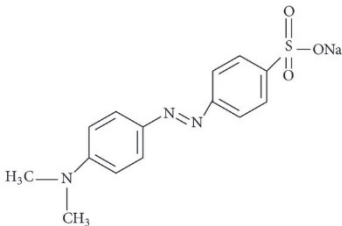
The experimental design for MO removal in this study consisted of three sub-experiments, namely i) sorption, ii) degradation, and iii) sorption-degradation (Table 1b).

Sorption of MO onto ACs

The AC with various concentrations of 770, 1384, and 1846 mg L^{-1} was put into 65 mL amber bottles (Fisher Scientific, USA) with Teflon-faced silicon septa (Kimble Chase, USA). They were then filled with MO solution with an initial concentration of 164 mg L^{-1} (equal to 335 mg-COD L^{-1}) without a headspace to prevent the loss of MO due to volatilization. The vials were horizontally shaken in an orbital shaker at 25°C and 200 rpm. At predetermined time intervals, the vials were removed from the shaker. Control experiments without AC (i.e., the MO solution-only) were also carried out to investigate

Table 1. a) Physicochemical properties of MO, b) kinetic experiments of sorption, degradation, and sorption-degradation of MO, c) physico-chemical properties of commercial AC and ZnCl₂-AC, and d) the first-order sorption rate constant of MO.

a)

Parameter	Structure/value
Molecular structure	
pKa	3.47
Molar mass (g mol ⁻¹)	327.33
Density (g cm ⁻³)	1.28
Solubility in water (mM)	15.3

Data obtained from: <https://pubchem.ncbi.nlm.nih.gov/compound/Methyl-orange>

b)

Sub-experiment	AC	PS	Fe ²⁺
Sorption	770-1846 mg L ⁻¹	-	-
Degradation	-	2592 mg L ⁻¹	378 mg L ⁻¹
Sorption-degradation	185-1846 mg L ⁻¹	346-3460 mg L ⁻¹	-

Note. AC = activated carbon, PS = persulfate solution, Fe²⁺ = Fe²⁺ solution
[MO] = 164 mg L⁻¹ (or 335 mg-COD L⁻¹). Temperature = 25°C. Shaking speed = 200 rpm.

c)

Parameter	Commercial AC	ZnCl ₂ -AC
BET surface area (A _{BET} , m ² g ⁻¹)	266.53	122.79
Pore size (Å)	13.5	20.7
d ₅₀ (µm)	39.05	28.58

d)

AC	Concentration (mg L ⁻¹)	k _{sorp} ⁰	C _e	R ²	SSE
Commercial AC	770	6.168	130.9	0.988	465.9
	1384	11.64	153.3	0.998	71.18
	1846	8.888	160.4	0.971	808.7
ZnCl ₂ -AC	770	7.404	133.3	0.990	369.2
	1384	5.439	138.4	0.989	385.3
	1846	3.360	194.4	0.987	234.7

Note. AC = activated carbon

Units: k_{sorp}⁰ = (h⁻¹) and C_e = (mg-COD L⁻¹)

the loss of MO due to natural degradation and adsorption onto glassware surfaces. Every experiment was conducted in duplicate.

Degradation of MO in the PS/Fe²⁺ System

A PS concentration of 2592 mg L⁻¹ and a Fe²⁺ concentration of 378 mg L⁻¹ were put into 65 mL amber bottles (Fisher Scientific, USA) with Teflon-faced silicon septa (Kimble Chase, USA). The same procedures as in Section 2.3.1 were then conducted. Control experiments without PS (i.e., the MO solution-only) were also carried out. Every experiment was conducted in duplicate.

Sorption-Degradation of MO in the PS/AC System

The AC and PS concentrations were varied to 4 variations, namely Variation 1: [AC] = 185 mg L⁻¹ and [PS] = 346 mg L⁻¹, variation 2: [AC] = 770 mg L⁻¹ and [PS] = 1728 mg L⁻¹, variation 3: [AC] = 1384 mg L⁻¹ and [PS] = 2592 mg L⁻¹, variation 4: [AC] = 1846 mg L⁻¹ and [PS] = 3460 mg L⁻¹. Each variation was put into 65 mL amber bottles (Fisher Scientific, USA) with Teflon-faced silicon septa (Kimble Chase, USA). Then, the same procedures as in Section 2.3.1 were conducted. Control experiments without AC and PS (i.e., the MO solution only) were also carried out. Every experiment was conducted in duplicate.

Analyses

Level of pH

The pH levels were recorded using a digital pH meter (Orion 3 Star pH Benchtop, Thermo Scientific, USA).

Concentration of COD in the MO Solution

The COD concentration in the MO solution was measured using the closed reflux-spectrophotometry method. Before the analysis, the liquid sample was filtered using a 0.45 μm polytetrafluoroethylene syringe filter (PTFE membrane, φ = 25 mm, Whatman, USA). Then, 2 mL of the filtered sample was immediately mixed with 2 mL of HACH COD reagent. The mixture was heated for 2 h at 150°C and cooled before analysis. After cooling, the mixture of aqueous samples and HACH reagents was analyzed using the HACH instrument to measure the COD concentration. Hence, the unit of the COD concentration in the MO solution was mg-COD L⁻¹.

HPLC-MS and ESR Analyses

The intermediate products of MO degradation were analyzed using an HPLC (Agilent Technologies, 1200 series, USA) coupled to a mass spectrometry system (Agilent 6410 QQQ, USA) with an electrospray interface as a supported ion source in the positive and negative

ion modes and connected to a Kinetex C18 column (100-mm length, 2.1 mm i.d., and 2.6 μm thickness, Phenomenex, USA) at 30°C. A linear gradient of the mobile phase comprised of 50% of a 0.1% formic acid solution (liquid chromatography grade, 99.9%, Merck, USA, solvent A) and 50% acetonitrile (liquid chromatography grade, LiChrosolv®, Germany, solvent B). The injection volume of the sample was 20 μL. The flow rate for the mobile phase was set at 0.3 mL min⁻¹. The additional parameters included the interface, and curved desolvation line voltages were 4.5 kV and 125 V, respectively; the nebulizer gas flow rate was 3 L min⁻¹; the drying gas flow rate was 10 L min⁻¹; the heat block temperature was 300°C; and the desolvation line temperature was 350°C [16]. The mass spectrometry system's quantitation limit was 1 ng mL⁻¹, with mass-to-charge (m/z) ratios of 100 and <2000 for the lower and upper limits, respectively.

The presence of radicals, such as superoxide radical (O₂⁻), was analyzed by mixing a 10-mL aqueous sample with 2 mL of 100 mM 5,5-dimethyl-1-pyrroline N-oxide (DMPO, 98.0%, Sigma-Aldrich, USA) or 2,2,6,6-tetramethylpiperidine (TEMP, 95%, Sigma-Aldrich, USA) as spin trapping reagents prepared in 10 mM phosphate buffer at pH 7 [25]. The radicals were identified using an electron spin resonance (ESR, JES-TE300, Jeol, Japan) spectrometer with the following conditions: a sweep width of 10 G, modulation amplitude of 250 G, modulation frequency of 100 KHz, microwave power of 2.0 mW, a resonance frequency of 9.42 GHz, a sweep time of 120 s, and a time constant of 100 ms.

Modeling

Since the first-order kinetic model is associated with surface-reaction kinetics, it was employed to match the sorption data [26, 27]. The equation of the model is shown in Eq. (1).

$$C(t) = C_0 e^{-k_{sorp}^0 t} + C_e (1 - e^{-k_{sorp}^0 t}) \quad (1)$$

where $C(t)$, C_0 , and C_e are the MO concentration (mg-COD L⁻¹) at time t (h), time 0, and equilibrium, respectively. The k_{sorp}^0 is the first-order rate constant for sorption-only (h⁻¹). Generally, the MO is degraded by the reactive oxygen species produced from the activation of the oxidant. Since the amount of oxidant is excessive, the kinetic reaction follows the pseudo-first-order kinetics.



In general, the degradation kinetic model is presented in Eq. (3).

$$C(t) = C_0 e^{-k_{ps}^0 t} \quad (3)$$

where k_{ps}^0 is the lumped rate constant (h^{-1}), including oxidation [28, 29] and sorption [30], in the presence of AC-only.

In our previous research, a coupled sorption-oxidation kinetic model was developed [17]. The equation of the model is shown in Eq. (4).

$$C(t) = C_0 e^{-(k_{sorp} + k_{ps})t} + \frac{k_{sorp} C_e}{k_{sorp} + k_{k_{ps}}} \left(1 - e^{-(k_{sorp} + k_{ps})t} \right) \quad (4)$$

where k_{sorp} is the first-order sorption rate constant in the simultaneous presence of AC and PS (h^{-1}), and k_{ps} is the first-order oxidation rate constant in the simultaneous presence of PS and AC (h^{-1}). The commercial software package TableCurve 2D® (Version 5.1, SYSTAT Software, Inc.) was used to determine the kinetic model parameters.

Results and Discussion

Physico-Chemical Properties of Commercial AC and ZnCl₂-AC

The physico-chemical properties of commercial AC and ZnCl₂-AC, such as A_{BET} , pore size distribution, and particle size distribution, are shown in Table 1c). The A_{BET} of commercial AC (266.53 $\text{m}^2 \text{g}^{-1}$, Fig. 1a) was larger than that of ZnCl₂-AC (122.79 $\text{m}^2 \text{g}^{-1}$, Fig. 1b). However, the pore size of commercial AC (13.5 Å) was slightly lower than that of ZnCl₂-AC (20.7 Å).

The AC's morphologies resulting from SEM analysis are shown in Fig. 1(c-j). The particle size of commercial AC ranged from 10 to 50 μm (Figs 1(c-d)), whereas that of ZnCl₂-AC ranged from 20 to 500 μm (Figs 1(g-h)). Furthermore, the ZnCl₂-AC was more porous than commercial AC. The pore sizes of both commercial AC (Figs 1(e-f)) and ZnCl₂-AC (Figs 1(i-j)) were almost similar in the range of 20-30 μm , which were categorized as mesoporous. The SEM results were consistent with the DLS analysis (Fig. 2). The particle size distribution (d_{50}) of both commercial AC and ZnCl₂-AC was at 39.05 μm and 28.58 μm , respectively (Table 1c). During pyrolysis, ZnCl₂ evaporation caused more mesopores to form on the ZnCl₂-AC surface [23, 24]. This process also leads to the formation of a larger particle size of ZnCl₂-AC than the commercial AC due to the agglomeration after ZnCl₂ evaporation.

Sorption Kinetics of MO onto ACs

The MO kinetic sorptions onto ACs were conducted at various AC dosages (Figs 3(a-b)). For commercial AC, using AC concentrations of 770, 1384, and 1846 mg L^{-1} resulted in MO removal efficiencies of 58.3%, 56.8%, and 66.1%, respectively. Then, for ZnCl₂-AC, using AC concentrations of 770, 1384, and 1846 mg L^{-1} resulted

in MO removal efficiencies of 41.7%, 60.3%, and 64.1%, respectively. It shows that the removal efficiency of MO sorption increased as the AC dosage was enhanced from 770 mg L^{-1} to 1846 mg L^{-1} within 2 h, both for commercial AC (58.3-66.1%) and ZnCl₂-AC (42.9-64.1%). This shows that commercial AC resulted in a higher MO removal efficiency than ZnCl₂-AC because of the higher BET surface area of commercial AC than that of ZnCl₂-AC.

The sorption-only data fitted to the first-order sorption kinetic model (Eq. (1)), and the fitted model parameters are shown in Table 1d). The k_{sorp}^0 values of MO sorption onto commercial AC increased from 6.168 h^{-1} to 11.64 h^{-1} as the AC dosage increased from 770 mg L^{-1} to 1384 mg L^{-1} . However, the k_{sorp}^0 value reduced to 8.888 h^{-1} when the AC dosage was enhanced to 1846 mg L^{-1} . Meanwhile, for ZnCl₂-AC, the highest k_{sorp}^0 value was achieved at the AC dosage of 770 mg L^{-1} (7.404 h^{-1}). Furthermore, the k_{sorp}^0 values decreased as the AC dosage increased to 1846 mg L^{-1} . This finding showed that the optimum equilibrium of MO sorption onto commercial AC was achieved at the AC dosage of 1384 mg L^{-1} , whereas that onto ZnCl₂-AC was at the AC dosage of 770 mg L^{-1} . The difference in AC dosage for reaching the optimum sorption equilibrium was affected by the AC modification by ZnCl₂. The ZnCl₂ filled the AC mesopores, causing a decrease in the available active site. This condition leads to the competition between MO and ZnCl₂ for the active site, inhibiting MO sorption on the AC surface.

Sorption-Degradation Kinetics Using AC-Activated PS

The MO was treated in the PS/AC system using various AC and PS concentrations. Before the sorption-degradation kinetic experiment, the PS-only system was tested to investigate the effect of PS on MO removal. The preliminary experiment showed that the PS-only did not affect the MO concentration. Four variations of AC and PS concentrations were shown in Table 2a), and for commercial AC, variations 1, 2, 3, and 4 resulted in MO removal efficiencies of 73.6%, 93.9%, 90.1%, and 100%, respectively. Then, for ZnCl₂-AC, the use of AC concentrations of 770, 1384, and 1846 mg L^{-1} resulted in MO removal efficiencies of 100%, 94.4%, 89.9%, and 100%, respectively (Figs 3(c-d)). As the AC and PS concentrations increased from variation 1 to variation 4, the MO removal efficiencies increased in the range of 73.6-100% for commercial AC and 89.9-100% for ZnCl₂-AC within 2 h of reaction.

The surface functional group of activated carbon activates the persulfate and generates a sulfate radical ($\text{SO}_4^{\cdot-}$). The sulfate radical then attacks the water molecule to become a hydroxyl radical and initiates the chain reaction that generates other reactive oxygen species, such as superoxide radicals [31, 32].

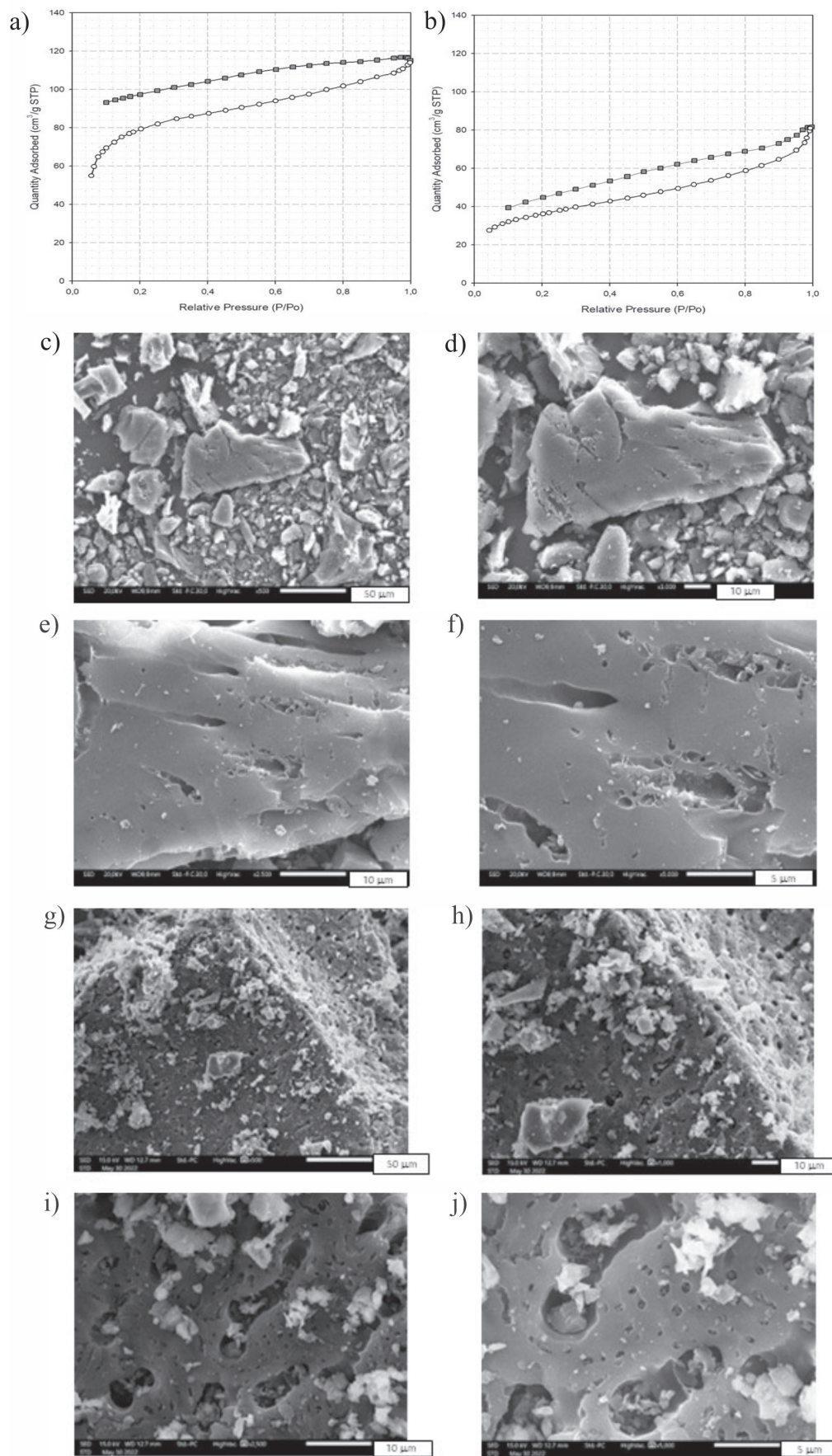


Fig. 1. A_{BET} adsorption-desorption isotherm profile of a) commercial AC and b) ZnCl₂-AC. Scanning electron microscopy (SEM) photographs of (c-f) commercial AC and (g-j) ZnCl₂-AC.

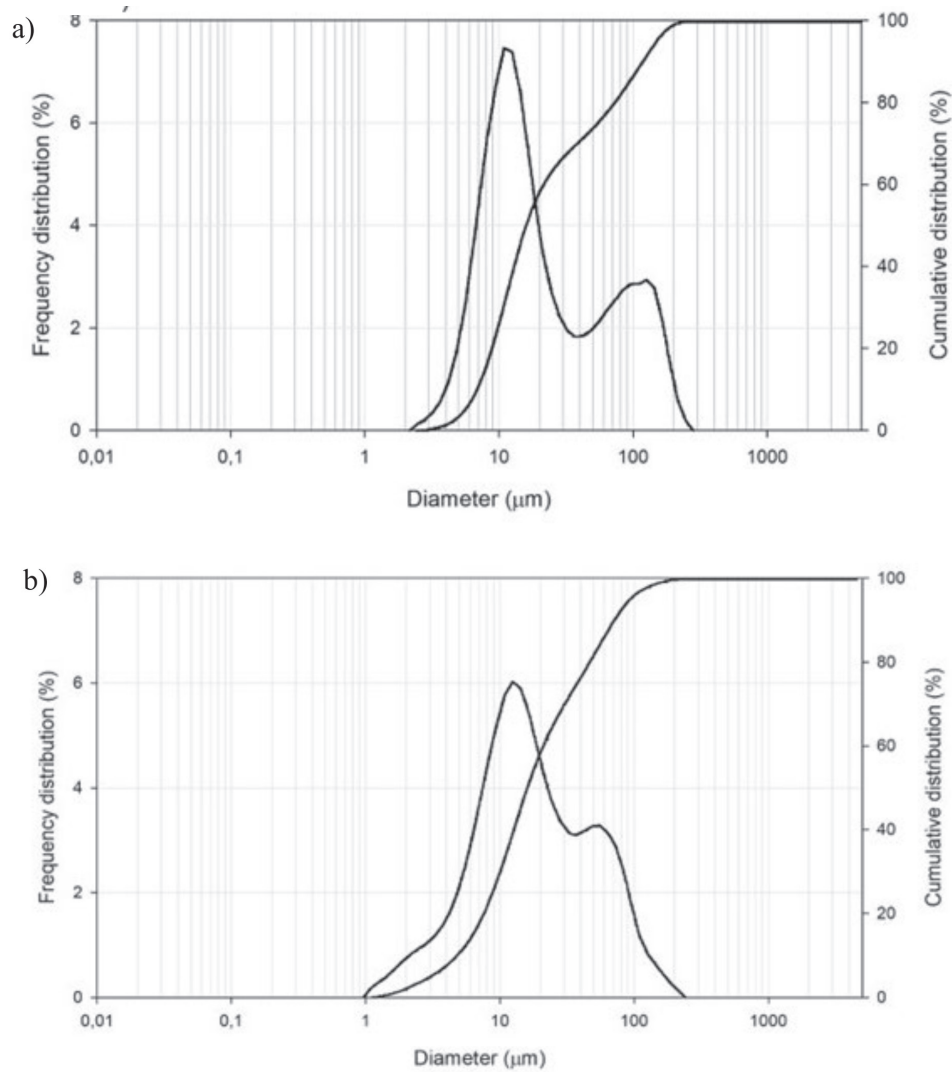
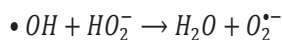
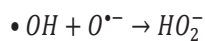
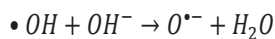
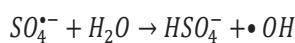
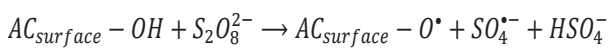


Fig. 2. Particle size distribution of a) commercial AC and b) ZnCl₂-AC.



In our previous study, Eq. (1) was combined with the degradation kinetic model (Eq. (2)), resulting in a coupled sorption-degradation kinetic model, as represented in Eq. (3) [17]. The experimental data of MO removal using AC-activated PS fitted to the coupled sorption-degradation kinetic model and the fitting model parameters are presented in Table 2a). In the PS/AC system, the removal mechanism was dominated by the oxidation by AC-activated PS compared to the sorption by AC-only, as indicated by the higher k_{PS} values than the k_{sorp} values, both for commercial AC ($k_{PS} = 5.058 - 6.447 \text{ h}^{-1}$, $k_{sorp} = 0.375 - 0.701 \text{ h}^{-1}$)

and ZnCl₂-AC ($k_{PS} = 4.703 - 5.601 \text{ h}^{-1}$, $k_{sorp} = 0.254 - 0.384 \text{ h}^{-1}$). Compared to the AC-only system, the presence of PS activated by AC almost transformed the removal mechanism completely from sorption to oxidation, as indicated by the drastic decrease of k_{sorp}^0 values, both for commercial AC (from $k_{sorp}^0 = 6.168 - 11.64 \text{ h}^{-1}$ to become $k_{sorp} = 0.375 - 0.701 \text{ h}^{-1}$) and ZnCl₂-AC (from $k_{sorp}^0 = 3.360 - 7.404 \text{ h}^{-1}$ to become $k_{sorp} = 0.254 - 0.384 \text{ h}^{-1}$). This result indicates that the PS/AC system enhanced the oxidation but depressed the sorption mechanism of MO removal. For commercial AC, the optimum MO removal (73.6%) was achieved at [MO] = 164 mg L⁻¹, [AC] = 185 mg L⁻¹, and [PS] = 346 mg L⁻¹. Meanwhile, for ZnCl₂-AC, the optimum MO removal (94.4%) was accomplished at [MO] = 164 mg L⁻¹, [AC] = 770 mg L⁻¹, and [PS] = 1728 mg L⁻¹. This result explains that using commercial AC for activating PS requires much less AC and PS dosages than using ZnCl₂-AC.

Table 2. a) The coupled sorption-degradation rate constant of MO and b) estimated cost for treating 2400 m³ of MO-containing wastewater.

a)

AC	Variation	AC concentration (mg L ⁻¹)	PS concentration (mg L ⁻¹)	k_{sorp}	k_{ps}	R ²	SSE
Commercial AC	1	185	346	0.701	6.447	0.997	188.2
	2	770	1728	0.456	5.782	0.984	1179
	3	1384	2592	0.375	6.546	0.997	263.6
	4	1846	3460	0.467	5.058	0.916	5859
ZnCl ₂ -AC	1	185	346	0.367	5.057	0.956	3321
	2	770	1728	0.384	5.601	0.995	465.7
	3	1384	2592	0.290	4.703	0.990	879.9
	4	1846	3460	0.254	5.120	0.961	2985

Note. AC = activated carbon

Units: k_{sorp} = (h⁻¹) and k_{ps} = (h⁻¹)

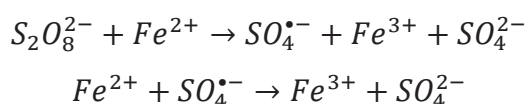
b)

	Amount	Price per Kg (USD)	Total Price (USD)
Commercial AC	185 g × 2400 m ³ = 444 kg	3.87	1,721
Potassium persulfate	346 g × 2400 m ³ = 830.4 kg	1.87	1,555
Total cost			3,271
Total cost per m ³ wastewater			1.36

Comparison of MO Removal Using PS/AC, AC-only, and PS/Fe²⁺ Systems

The MO removal efficiency of different systems (PS/AC, AC-only, and PS/Fe²⁺) was compared. In the PS/Fe²⁺ system, our previous study showed that the optimum molar ratio of PS:Fe²⁺ for oxidizing phenol was achieved at the PS:Fe²⁺ of 2:1 [16]. Therefore, this PS:Fe²⁺ molar ratio was used in this study. The change in MO concentrations during the PS/AC, AC-only, and PS/Fe²⁺ systems is shown in Figs 3(e-f). In summary, for commercial AC, the MO removal efficiencies were in the order of PS/AC (90.1%)>AC-only (56.8%)>PS/Fe²⁺ (23.8%) within 2 h. Meanwhile, for ZnCl₂-AC, the MO removal efficiencies were in the order of PS/AC (89.9%)>AC-only (60.3%)>PS/Fe²⁺ (23.8%) within 2 h (Figs 3(e-f)). These results indicated that the PS/AC system showed the best performance in removing MO compared to the AC-only and PS/Fe²⁺ systems, where the commercial AC showed a slightly better performance than the ZnCl₂-AC.

Activated carbon performs better in activating persulfate than iron. This may be due to iron itself scavenging sulfate radicals [33].



Previous studies reported that AC could effectively activate PS for the degradation of organic compounds, such as acetaminophen, sulfamethoxazole, and nitrophenol [21, 34, 35]. Acetaminophen concentration was significantly reduced when activated carbon was applied in persulfate oxidation [21, 34], demonstrating a more significant removal of sulfamethoxazole in the PS+AC system compared with AC only. Similar results were also observed by [35], in which the removal of nitrophenol could be enhanced by activated carbon addition in the persulfate process. The highly porous surface of activated carbon could act as an electron-transfer mediator in activating persulfate, generating sulfate radicals, which results in the effective degradation of organic compounds.

Radical Investigation

The presence of radical species was investigated using an ESR spectrometer coupled with 5,5-dimethyl-1-pyrroline N-oxide (DMPO) as a spin-trapping agent. Figs 3(g-h) show the ESR analysis results. A control experiment was conducted by analyzing PS-only (Figs 3(g-h)); black line); no radical signal was detected. In the Figure, the DMPO-O₂^{•-} signal appeared, whereas no other signal was discovered. This result is consistent with our previous study, revealing the presence of O₂^{•-} as the predominant radical species generated from the

PS activation by AC material (i.e., colloidal AC) [16]. In addition, the intensity of the DMPO- $O_2^{\cdot-}$ signal generated from commercial AC-activated PS was higher than that from $ZnCl_2$ -AC-activated PS. This result indicated that the $O_2^{\cdot-}$ was the dominant radical species

in the PS/AC system. The commercial AC produced more $O_2^{\cdot-}$ than the $ZnCl_2$ -AC because the commercial AC has larger active sites for generating $O_2^{\cdot-}$ from PS than the $ZnCl_2$ -AC.

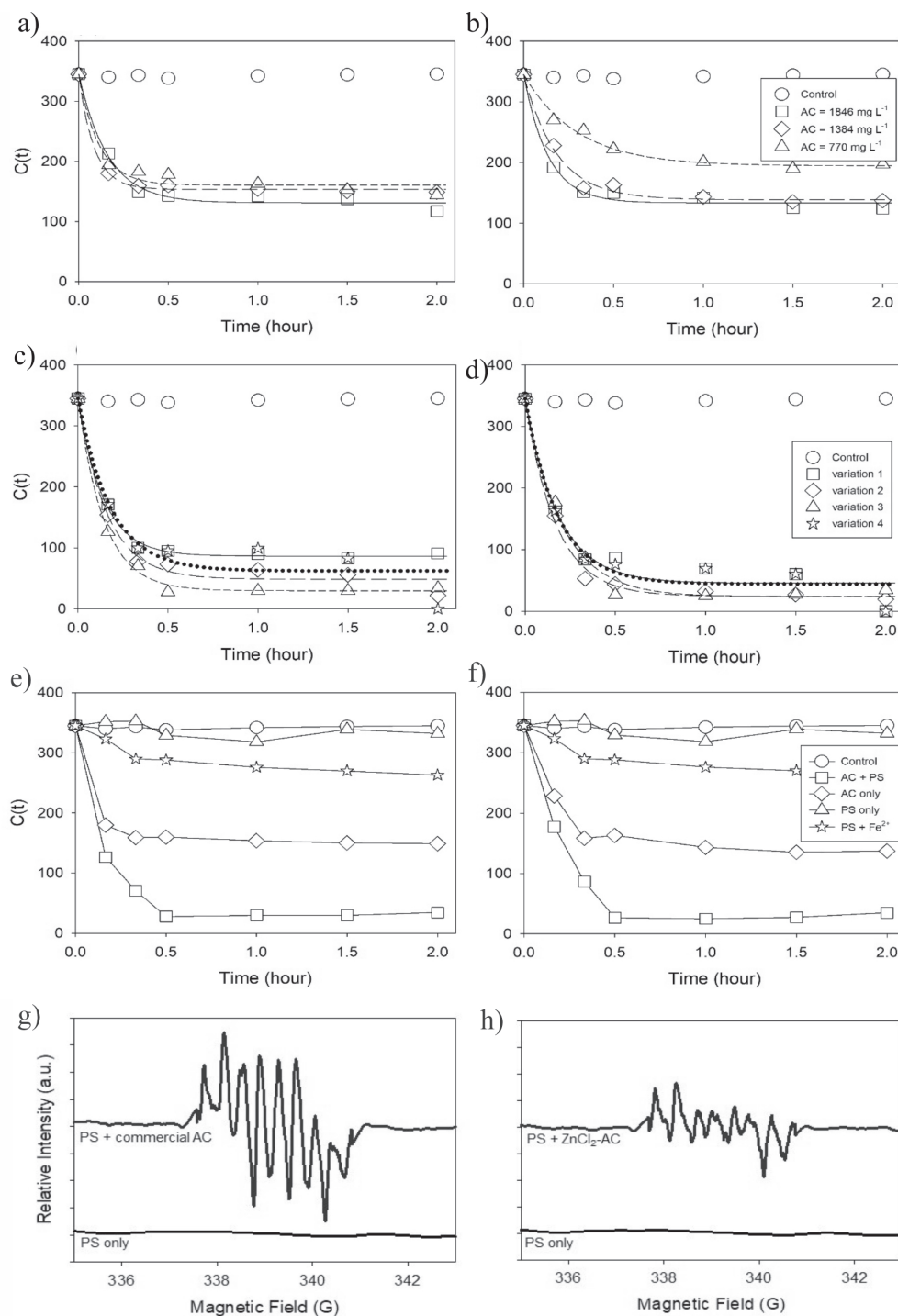


Fig. 3. Sorption kinetic of MO using a) commercial AC and b) $ZnCl_2$ -AC ([AC] = 770, 1384, and 1846 mg L⁻¹), sorption-degradation of MO in the PS/AC system c) commercial AC and d) $ZnCl_2$ -AC (Variation 1: [AC] = 185 mg L⁻¹ and [PS] = 346 mg L⁻¹; variation 2: [AC] = 770 mg L⁻¹ and [PS] = 1728 mg L⁻¹; variation 3: [AC] = 1384 mg L⁻¹ and [PS] = 2592 mg L⁻¹; variation 4: [AC] = 1846 mg L⁻¹ and [PS] = 3460 mg L⁻¹), MO removal at various system e) commercial AC and f) $ZnCl_2$ -AC ([AC] = 1384 mg L⁻¹, [PS] = 2592 mg L⁻¹, and [Fe²⁺] = 378 mg L⁻¹), and ESR spectra in the PS/AC system g) commercial AC and h) $ZnCl_2$ -AC ([AC] = 1384 mg L⁻¹, [PS] = 2592 mg L⁻¹, and [DMPO] = 100 mM in 10 mM phosphate buffer at pH 7). [MO] = 164 mg L⁻¹. $C(t)$ is MO concentration (mg-COD L⁻¹). Reaction time was within 2 h at 25°C and 200 rpm.

Analysis of Byproducts and Degradation Pathways

The byproducts of MO degradation in the PS/AC system were identified using HPLC–MS with an electrospray interface as a supported ion source in

positive and negative ion modes. The analysis results are shown in Fig. 4. The initial MO components were detected at m/z of 372, as depicted in Fig. 4a). The predominant product component from the PS/AC system was detected at m/z of 104 (Fig. 4b), referred to as hydroxyl aniline or aminophenol [36, 37]. Fig. 4c) shows

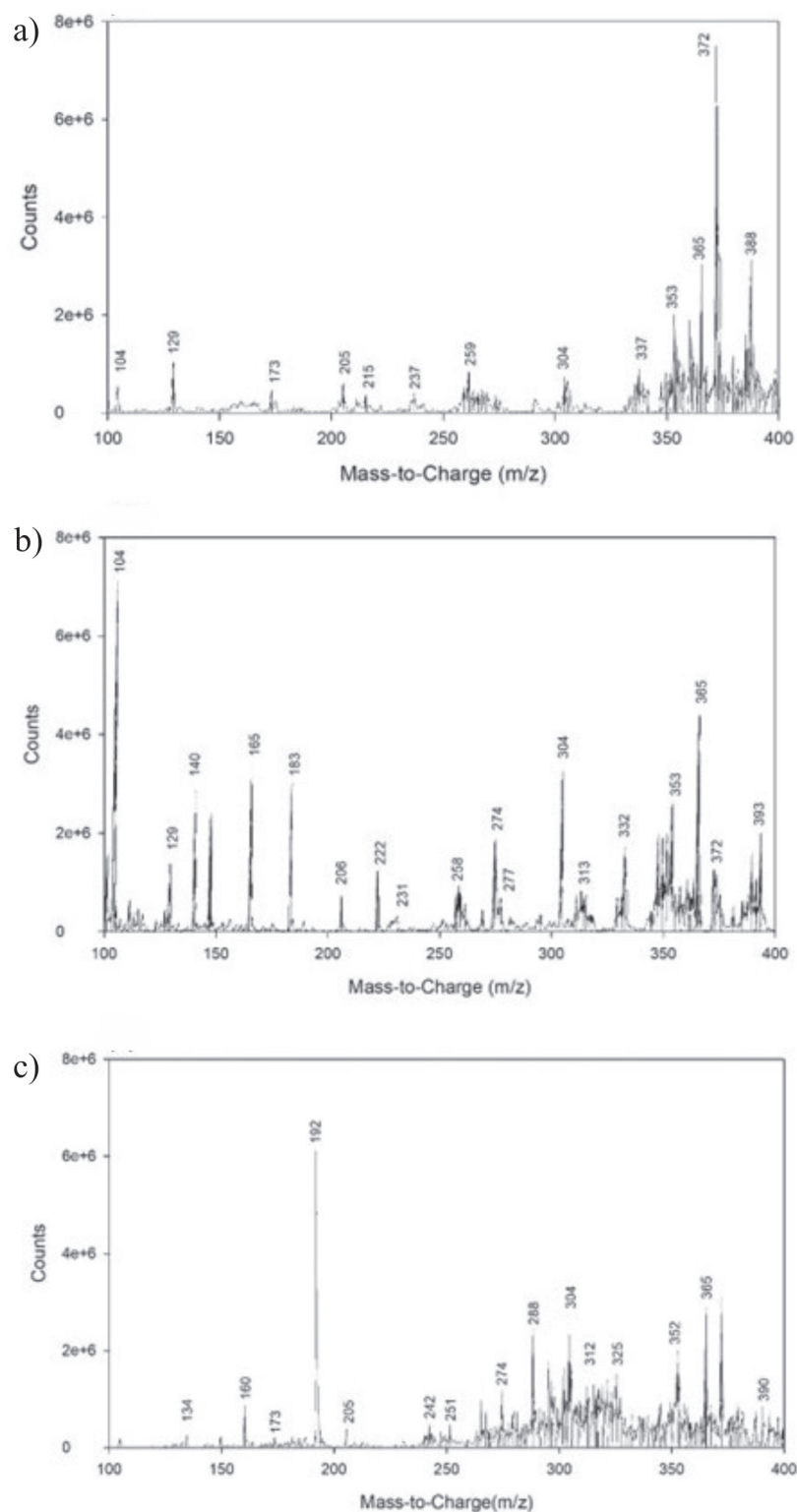


Fig. 4. LC–MS analyses of MO a) before oxidation, and byproduct after oxidation in the PS/AC system using b) commercial AC and c) ZnCl₂-AC. [MO] = 164 mg L⁻¹, [AC] = 1384 mg L⁻¹, [PS] = 2592 mg L⁻¹.

the predominant product component of MO degradation has m/z of 192.

The MO degradation pathway is proposed in Fig. 5. Here, the hydroxyl aniline could be formed via the asymmetric breakage of MO. Precedingly, the asymmetric cleavage of the MO chain structure formed 2 components of 4-dimethylamino phenol (E, $m/z = 140$) and 4-diazenylbenzene sulfonic acid (G, $m/z = 183$) [38]. The nitrogen double bond in 4-diazenylbenzene sulfonic acid, then broke to form the component sulfanilic acid (H, $m/z = 173$) and continued to form benzene sulfonic acid (I, $m/z = 165$). Meanwhile, the demethylation of 4-dimethylamino phenol produced hydroxyl aniline compound (F, $m/z = 104$) as the predominant product. The detection band at $m/z = 304$ to 393 was from hydroxylation, followed by successive demethylation of the MO compound. The hydroxylated MO (J, $m/z = 313$), then demethylated (K, $m/z = 304$), dehydroxylated (L, $m/z = 274$), and deaminated (M, $m/z = 258$) before the removal of its aromatic ring to become 4-diazenylbenzene sulfonic acid (G, $m/z = 183$) [39]. The byproduct at m/z of 192 may come from the linear chain of $\text{COOH}(\text{CH}_2)_5\text{N}(\text{COOH})(\text{OH})$ that is depicted as component D ($m/z = 183$) [40]. The carboxylation of demethylated MO (B, $m/z = 304$) formed the carbonylated MO (C, $m/z = 258$) before opening its ring to become $\text{COOH}(\text{CH}_2)_5\text{N}(\text{COOH})(\text{OH})$. Overall, the intermediate products from ring opening, demethylation, azo bond breakage, and aromatic ring removal processes were converted to carbon dioxide and water.

Potential Application of PS/AC System for Wastewater Treatment in the Textile Industry

The use of the PS/AC system for MO removal in textile industries was estimated based on the optimum kinetic experiments (Figs 3(a-b) and Table 2a). Based on the results in Figs 3(a-b), the commercial AC was better than $\text{ZnCl}_2\text{-AC}$ for MO degradation on the industrial scale because the highest k_{orp} and k_{PS} values were achieved at the lowest AC and PS dosages ($[\text{PS}] = 346 \text{ mg L}^{-1}$, $[\text{AC}] = 185 \text{ mg L}^{-1}$), where the MO removal efficiency achieved 85% within 30 min.

For every 1 m^3 of MO-containing wastewater, 185 g of commercial AC and 346 g of potassium persulfate are needed. On average, for every 1 ton of textile product, around 200-300 m^3 of freshwater is used [5], where 3000 m^3 of freshwater will be used to produce 10 tons of textile. Uddin et al. [5] reported that about 80% of the freshwater used in the production process is converted to wastewater, which equals 2400 m^3 of MO-containing wastewater. Recently, the quality standard for disposing of treated textile wastewater in Indonesia includes COD at a maximum concentration of 250 mg L^{-1} [41]. In this study, the initial MO concentration of 164 mg L^{-1} equals 335 mg L^{-1} COD, which is above the maximum COD standard for discharge to the environment. To reduce 85% of COD concentration (i.e., up to 50 mg L^{-1} COD based on our kinetic study), the estimated cost for treating 2400 m^3 of MO-containing wastewater with commercial AC and potassium persulfate is approximately IDR 50,721,600 (USD 3,270) or equal to IDR 21,134 (USD 1.36) per m^3 of wastewater (Table 2b).

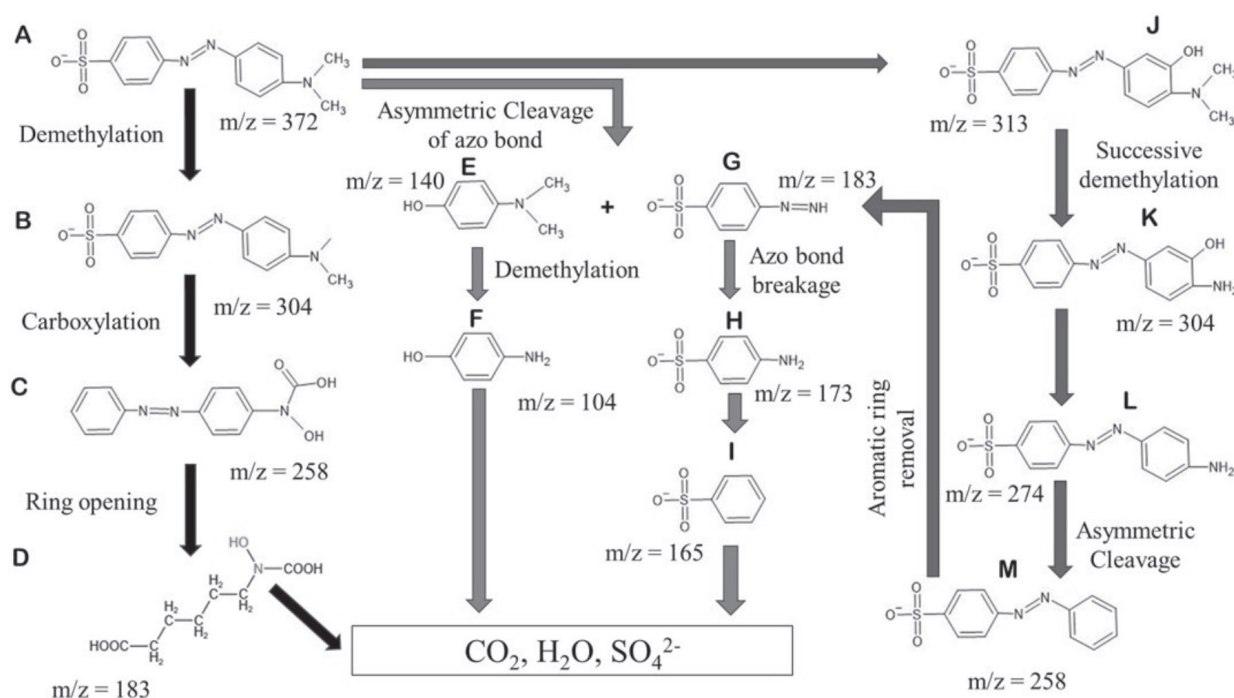


Fig. 5. Degradation pathway of MO in water by PS/AC system.

The calculation is estimated in a batch system with a removal efficiency of 85% within 30 min. In industrial applications, the continuous stirred tank reactor (CSTR) is the best candidate for MO-containing wastewater treatment, equipped with mixing and sedimentation tanks. The CSTR is a cylindrical shape with a diameter

of 8 m and a height of 4 m, resulting in an area of 50 m² and a volume of 200 m³. Therefore, this reactor can handle 2400 m³ of wastewater within 12 h of operational time.

In comparison, an active sludge through biological reaction can be used as an alternative to treat MO.

Table 3. Comparison of removal efficiencies of dye in this study and the other studies

No.	Removal mechanism	Optimum condition	Removal efficiency (%)	Ref.
1	MO	$C_0 = 164 \text{ mg L}^{-1}$ Commercial AC = 185 mg L ⁻¹ $PS = 346 \text{ mg L}^{-1}$ Temp = 25°C t = 1 h and $C_0 = 164 \text{ mg L}^{-1}$ $ZnCl_2\text{-AC} = 770 \text{ mg L}^{-1}$ $PS = 1728 \text{ mg L}^{-1}$ Temp = 25°C t = 1 h	91.3 (commercial AC) and 92.1 (ZnCl ₂ -AC)	This study
2	Antraquinone, i.e., Acid Blue 129	$C_0 = 25 \text{ mg L}^{-1}$ PDS/PMS = 2.50 mM $UV = 416 \text{ kWh m}^{-3} \text{ order}^{-1}$ Temp = 21°C t = 15 min	88	[43]
3	Methylene blue (MeB), methyl orange (MeO), rhodamin B (RhB)	$C_0 = 30 \text{ }\mu\text{M}$ $PS = 1 \text{ mM}$ $UV = 250 \text{ }\mu\text{W cm}^{-2}$ Temp = 25°C t = 15 min	100	[44]
4	Acid orange 7 (AO7)	$C_0 = 50 \text{ mg L}^{-1}$ Biochar = 1 g L ⁻¹ PDS = 20 mM pH = 6 Temp = 25°C t = 20 min	98–99.2	[45]
5	Brilliant green (BG), eosin yellow (EY)	$C_0 = 10 \text{ mg L}^{-1}$ Catalyst (PWC) = 2 g L ⁻¹ $PMS = 2 \text{ g L}^{-1}$ Temp = 25°C t = 2 h	100	[46]
6	MO	$C_0 = 25 \text{ mg L}^{-1}$ $ZrO_2 = 1 \text{ g L}^{-1}$ $PS = 250 \text{ mg L}^{-1}$ pH = 7 Temp = 25°C t = 10 min	99	[47]
7	Disperse blue (DB), indigo blue (IB), reactive red (RR)	$C_0 = 25 \text{ mg L}^{-1}$ $FeSO_4 \cdot 7H_2O = 10 \text{ g L}^{-1}$ $PS = 8 \text{ g L}^{-1}$ pH = 7 Temp = 25°C t = 60 min	96.25–96.73	[48]
8	RB222	$C_0 = 25 \text{ mg L}^{-1}$ Fenton = 0.17 g L ⁻¹ $PMS = 0.1 \text{ g L}^{-1}$ pH = 6.5 Temp = 25°C t = 60 min	85.66	[49]

However, the biological process requires a long retention time of around 19-48 h [42]. This reaction is 40 times longer than the AC sorption process, requiring a 40 times wider area of the 50 m²-CSTR. Therefore, using AC combined with PS is the best choice in the limited industrial area. Various methods, such as biological regeneration, wet oxidation regeneration, solvent regeneration, electrochemical regeneration, and catalytic wet oxidation, can regenerate the saturated AC in the CSTR reactor.

Limitations of this Study and Future Prospects of PS/AC System for Research and Industrial Application

Indonesia's government aims to promote green technology in all industrial fields. Wastewater treatment technology is one of the targets that is being addressed by developing sophisticated technology, and its application does not require large areas of land. As the rate of industrialization increases and the population increases, area or land becomes expensive. For this reason, future research prospects will be more concentrated on wastewater treatment technology that can reduce pollutants in a relatively short time, such as research on applying plasma technology, advanced oxidation processes (AOPs), and chemical and electrochemical processes. The research in this paper uses active carbon and persulfate, which have been proven to reduce MO in a short time. Using activated carbon to reduce MO compounds is not limited to textile wastewater but can also be applied to treat wastewater from the paper industry, leather tannery, and food industry because this industrial wastewater also contains MO compounds. The removal efficiency of MO was compared to those in other studies of dye removal, as shown in Table 3 [43-49]. The experimental research in this study is still superior in terms of removal efficiency, usability, and low cost compared to other studies about dye removal using sorption or oxidation.

One of the interesting things in this study is the application of Indonesian palm kernel shell-based activated carbon (ZnCl₂-AC) as an activator for PS in removing MO. However, the use of commercial AC still gave a higher performance than ZnCl₂-AC for MO degradation because it required a lower dosage than the use of ZnCl₂-AC. Even so, the results of this study are essential for the next research. The characteristics of Indonesian palm kernel shell-based activated carbon need to be improved by investigating the operating conditions of the pyrolysis and activation process. When the characteristics of the Indonesian palm kernel shell-based-activated carbon improve, it can be more suitable as an activator for PS in treating MO pollutants. In addition, the other operating conditions in the persulfate-based advanced oxidation process need to be optimized to get the highest MO removal efficiency, such as temperature and agitation speed. Researchers worldwide are currently developing advanced and effective water/

wastewater treatments that are suitable for development in various countries. The results of this research can be used to create a wealth of knowledge and research.

Conclusions

The use of commercial AC and ZnCl₂-AC combined with PS to remove MO in water was investigated. The PC/AC system was superior in removing MO compared to AC-only and PS/Fe²⁺ systems. In the PC/AC system, the commercial AC was more advantageous than the ZnCl₂-AC for MO removal due to the lower dosage of commercial AC. The optimum removal condition for commercial AC was achieved at [MO] = 164 mg L⁻¹ (or 335 mg-COD L⁻¹) [AC] = 185 mg L⁻¹, and [PS] = 346 mg L⁻¹, and for ZnCl₂-AC was accomplished at [MO] = 164 mg L⁻¹ (or 335 mg-COD L⁻¹), [AC] = 770 mg L⁻¹, and [PS] = 1728 mg L⁻¹. The individual sorption fitted to the first-order kinetic model, whereas the sorption/degradation data followed the coupled sorption-oxidation kinetic model. The PS/AC system enhanced the oxidation mechanism but depressed the sorption mechanism, as indicated by higher k^0_{sorp} values than the k_{sorp} values. Moreover, the O₂⁻ radical species contributed dominantly to the oxidation mechanism. The HPLC-MS detected various byproducts, indicating several degradation pathways, such as demethylation, carboxylation, ring opening, azo bond breakage, asymmetric cleavage, and aromatic ring removal, before mineralizing MO to carbon dioxide and water. In addition, the use of commercial AC combined with PS is estimated to be suitable for MO removal on an industrial scale compared to the biological process, attributed to the rapid removal time. The results of this study have crucial implications for wastewater treatment in textile industries by utilizing radical species from AC-activated PS for various dye contaminants. In the future, the application of this study will be one of the best options for wastewater treatment, especially in textile industries.

Acknowledgments

This research was supported by the RIIM LPDP Grant and BRIN, grant number (B-840/II.7.5/FR.06/5/2023 and B-977/III.5/FR.06.00/5/2023). We also thank to the Research Organization for Life Sciences and Environment/Research Center for Environmental and Clean Technology and the Graduate School of Environmental Studies Diponegoro University.

Conflict of Interest

The authors declare no potential conflict of interest regarding the publication of this work.

References

1. ESTIKARINI H.D., HADIWIDODO M., LUVITA V. Penurunan Kadar COD dan TSS pada limbah tekstil dengan metode ozonasi. *Jurnal Teknik Lingkungan*, **5**, 1, **2016**.
2. AZANAW A., BIRLIE B., TESHOME B., JEMBERIE M. Textile effluent treatment methods and eco-friendly resolution of textile wastewater. *Case Studies in Chemical and Environmental Engineering*, **6**, 100230, **2022**.
3. RASHID T., IQBAL D., HAZAFA A., HUSSAIN S., SHER F., SHER F. Formulation of zeolite supported nano-metallic catalyst and applications in textile effluent treatment. *Journal of Environmental Chemical Engineering*, **8** (4), 104023, **2020**.
4. ALMAAMARY E.A.S., ABDULLAH S.R.S., ISMAIL N. 'I., IDRIS M., KURNIAWAN S.B., IMRON M.F. Comparative performance of Scirpus grossus for phytotreating mixed dye wastewater in batch and continuous pilot subsurface constructed wetland systems. *Journal of Environmental Management*, **307**, 114534, **2022**.
5. UDDIN M.A., BEGUM M.S., ASHRAF M., AZAD A.K., ADHIKARY A.C., HOSSAIN M.S. Water and chemical consumption in the textile processing industry of Bangladesh. *PLOS Sustainability and Transformation*, **2**, 1, **2023**.
6. AHMAD M., QURESHI M.T., REHMAN W., ALOTAIBI N.H., GUL A., HAMEED R.S.A., AL ELAIMI M., ABD EL-KADER M.F.H., NAWAZ M., ULLAH R. Enhanced photocatalytic degradation of RhB dye from aqueous solution by biogenic catalyst Ag@ZnO. *Journal of Alloys and Compounds*, **895** (2), 162636, **2022**.
7. HOJJATI-NAJAFABADI A., FARAHBAKHS V., GHOMALIAN G., FENG P., DAVAR F., AMINABHAVI T.M., VASSEGHIAN Y., KAMYAB H., RAHIMI H. Controllable synthesis of nanostructured flower-like cadmium sulfides for photocatalytic degradation of methyl orange under different light sources. *Journal of Water Process Engineering*, **59**, 105002, **2024**.
8. PANCHAL D., SHARMA A., PAL S. 1 – Novel photocatalytic techniques for organic dye degradation in water. *Photocatalytic Degradation of Dyes: Current Trends and Future Perspectives*, **1**, **2021**.
9. AZHA S.F., ISMAIL S. Feasible and economical treatment of real hand-drawn batik/textile effluent using zwitterionic adsorbent coating: Removal performance and industrial application approach. *Journal of Water Process Engineering*, **41**, 102093, **2021**.
10. CHOONG C.E., IBRAHIM S., BASIRUN W.J. Mesoporous silica from batik sludge impregnated with aluminum hydroxide for the removal of bisphenol A and ibuprofen. *Journal of Colloid and Interface Science*, **541**, 12, **2019**.
11. SULISTYANINGSIH T., SARI D.A., WIDIARTI N., ASTUTI W., WULANDARI R., HARJUNOWIBOWO D. Green synthesis of gaharu leaf extract-modified magnetite as an adsorbent for methyl orange textile dyes. *Waste Management Bulletin*, **2** (1), 327, **2024**.
12. LAHIRI S.K., ZHANG C., SILLANPAA M., LIU L. Nanoporous NiO@SiO₂ photo-catalyst prepared by ion-exchange method for fast elimination of reactive dyes from wastewater. *Materials Today Chemistry*, **23**, 100677, **2022**.
13. LUVITA V., SUGIARTO A.T., BISMO S. Characterization of dielectric barrier discharge reactor with nanobubble application for industrial water treatment and depollution. *South African Journal of Chemical Engineering*, **40**, 246, **2022**.
14. MA S., KIM K., CHUN S., MOON S.Y., HOONG Y. Plasma-assisted advanced oxidation process by a multi-hole dielectric barrier discharge in water and its application to wastewater treatment. *Chemosphere*, **243**, 125377, **2020**.
15. SEPTIAN A., AL MASUD M.A., NUGROHO R., SHIN W.S. Evaluating the potential of wax impregnated reactive components for long-term acenaphthene removal. *Journal of Water Process Engineering*, **56**, 104466, **2023**.
16. SEPTIAN A., KUMAR A.V.N., SIVASANKAR A., CHOI J., HWANG I., SHIN W.S. Colloidal activated carbon as a highly efficient bifunctional catalyst for phenol degradation. *Journal of Hazardous Materials*, **414**, 125474, **2021**.
17. SEPTIAN A., SHIN W.S. Slow-release persulfate candle-assisted electrochemical oxidation of 2-methylnaphthalene: Effects of chloride, sulfate, and bicarbonate. *Journal of Hazardous Materials*, **400**, 123196, **2020**.
18. ANNAMALAI S., SEPTIAN A., CHOI J., SHIN W.S. Remediation of phenol contaminated soil using persulfate activated by ball-milled colloidal activated carbon. *Journal of Environmental Management*, **310**, 114709, **2022**.
19. CHEN J., QIAN Y., LIU H., HUANG T. Oxidative degradation of diclofenac by thermally activated persulfate: implication for ISCO. *Environmental Science and Pollution Research*, **23**, 3824, **2016**.
20. KIM D.G., PHAM V.L., KO S.O. Catalytic effects of activated-carbon particle size on the oxidative degradation mechanisms of a pharmaceutical. *Journal of Environmental Chemical Engineering*, **10**, 107179, **2022**.
21. LEE Y., LI Y., CHEN M., CHEN Y., KUO J., LO S. Efficient decomposition of perfluorooctanoic acid by persulfate with iron-modified activated carbon. *Water Research*, **174**, 115618, **2020**.
22. NABILA R., HIDAYAT W., HARYANTO A., HASANUDIN U., IRYANI D.A., LEE S., KIM S., KIM S., CHUN D., CHOI H., IM H., LIM J., KIM K., JUN D., MOON J., YOO J. Oil palm biomass in Indonesia: Thermochemical upgrading and its utilization. *Renewable and Sustainable Energy Reviews*, **176**, 113193, **2023**.
23. HOCK P.E., ZAINI M.A.A. Activated carbons by zinc chloride activation for dye removal – a commentary. *Acta Chimica Slovaca*, **11**, 99, **2018**.
24. HUSSARO K. Preparation of activated carbon from palm oil shell by chemical activation with Na₂CO₃ and ZnCl₂ as impregnated agents for H₂S adsorption. *American Journal of Environmental Sciences*, **10**, 336, **2014**.
25. LEE H., LEE H.J., JEONG J., LEE J., PARK N.B., LEE C. Activation of persulfates by carbon nanotubes: Oxidation of organic compounds by nonradical mechanism. *Chemical Engineering Journal*, **266**, 28, **2015**.
26. GENC N., DOGAN E.C. Adsorption kinetics of the antibiotic ciprofloxacin on bentonite, activated carbon, zeolite, and pumice. *Desalination and Water Treatment*, **53**, 785, **2015**.
27. MA J., LEI Y., KHAN M.A., WANG F., CHU Y., LEI W., XIA M., ZHU S. Adsorption properties, kinetics & thermodynamics of tetracycline on carboxymethyl-chitosan reformed montmorillonite. *International Journal of Biological Macromolecules*, **124**, 557, **2019**.
28. ZHAI J., WANG Q., LI Q., SHANG B., RAHAMAN M.H., LIANG J., JI J., LIU W. Degradation mechanisms of carbamazepine by δ-MnO₂: Role of protonation of degradation intermediates. *Science of the Total Environment*, **640–641**, 981, **2018**.

29. KUAN W.H., HU C.Y., LIU B.S., TZOU Y.M. Degradation of antibiotic amoxicillin using 1×1 molecular sieve-structured manganese oxide. *Environmental Technology*, **34**, 2443, **2013**.
30. JIANG W.-T., CHANG P.-H., WANG Y.-S., TSAI Y., JEAN J.-S., LI Z. Sorption and desorption of tetracycline on layered manganese dioxide birnessite. *International Journal of Environmental Science and Technology*, **12**, 1695, **2015**.
31. LEE Y.-C., LO S.-L., KUO J., HUANG C.-P. Promoted degradation of perfluorooctanoic acid by persulfate when adding activated carbon. *Journal of Hazardous Materials*, **261**, 463-469, **2013**.
32. SUGIHARTONO V.E., MAHASTI N.N.N., SHIH Y.-J., HUANG Y.-H. Photo-persulfate oxidation and mineralization of benzoic acid: Kinetics and optimization under UVC irradiation. *Chemosphere*, **296**, 133663, **2022**.
33. KARIM A.V., JIAO Y., ZHOU M., NIDHEESH P.V. Iron-based persulfate activation process for environmental decontamination in water and soil. *Chemosphere*, **265**, 129057, **2021**.
34. LIANG J., XU X., ZAMAN W.Q., HU X., ZHAO L., QIU H., CAO X. Different mechanisms between biochar and activated carbon for the persulfate catalytic degradation of sulfamethoxazole: Roles of radicals in solution or solid phase. *Chemical Engineering Journal*, **375**, 121908, **2019**.
35. RODRIGUES C.S.D., AZIZ S.N.A., PEREIRA M.F.R., SOARES O.S.G.P., MADEIRA L.M. Degradation of p-Nitrophenol by activated persulfate with carbon-based materials. *Journal of Environmental Management*, **343**, 118140, **2023**.
36. KONG X., ZHU H., CHEN C., HUANG G., CHEN Q. Insights into the reduction of 4-nitrophenol to 4-aminophenol on catalysts. *Chemical Physical Letters*, **684**, 148, **2017**.
37. XU J.-Z., MIAO J.-J., LIN H., DING T., ZHAO Z.-Y., WU B., SHEN C.-Y., JIANG Y. Determination of amitraz and 2,4-dimethylaniline residues in honey by using LC with UV detection and MS/MS. *Journal of Separation Science*, **32** (23–24), 4020, **2009**.
38. LIU W., LIU C., LIU L., YOU Y., JIANG J., ZHOU Z., DONG Z. Simultaneous decolorization of sulfonated azo dyes and reduction of hexavalent chromium under high salt condition by a newly isolated salt-tolerant strain *Bacillus circulans* BWL1061. *Ecotoxicology and Environmental Safety*, **141**, 9, **2017**.
39. AN Q., TANG M., DENG S., JIAO Y., LIU C., YANG M., YE Z., ZHAO B. Methyl orange degradation with peroxydisulfate activated with the synergistic effect of the acid-modified red mud and biochar catalyst. *Arabian Journal for Science and Engineering*, **48**, 8819, **2023**.
40. TANTUVOY S., KUMAR M., NAMBI I. Microwave assisted zirconium oxide based catalytic activation of persulfate for methyl orange dye degradation. *Journal of Environmental Chemical Engineering*, **11** (5), 110721, **2023**.
41. HITCHENS D.M., CLAUSEN J., FICHTER K. *International Environmental Management Benchmarks: Best Practice Experiences from America, Japan and Europe*; Klaus Fitcher, Eds., Springer: New York, USA, **1999**.
42. YANG X., LOPEZ-GRIMAU V., VILASECA M., CRESPI M. Treatment of textile wastewater by CAS, MBR, and MBBR: A comparative study from technical, economic, and environmental perspectives. *Water*, **12** (5), 1306, **2020**.
43. RAMAKRISHNAN R.K., VENKATESHAIAH A., GRUBEL K., KUDLEK E., SILVESTRI D., PADIL V.V.T., GHANBARI F., CERNIK M., WACLAWEK S. UV-activated persulfates oxidation of anthraquinone dye: Kinetics and ecotoxicological assessment. *Environmental Research*, **229**, 115910, **2023**.
44. HOANG N.T., NGUYEN V.T., TUAN N.D.M., MANH T.D., LE P.-C., TAC D.V., MWAZIGHE F.M. Degradation of dyes by UV/Persulfate and comparison with other UV-based advanced oxidation processes: Kinetics and role of radicals. *Chemosphere*, **298**, 134197, **2022**.
45. LI Z., DENG S., AN Q., ZHAO B., YANG Z., XU B., ZHANG W. Enhanced activation of persulfate by modified red mud biochar for degradation of dye pollutant: Resource utilization and non-radical activation. *Journal of Environmental Management*, **353**, 120181, **2024**.
46. KUMAR S., TEWARI C., SAHOO N.G., PHILIP L. Mechanistic insights into carbo-catalyzed persulfate treatment for simultaneous degradation of cationic and anionic dye in multicomponent mixture using plastic waste-derived carbon. *Journal of Hazardous Materials*, **435**, 128956, **2022**.
47. TANTUVOY S., KUMAR M., NAMBI I. Microwave assisted zirconium oxide based catalytic activation of persulfate for methyl orange dye degradation. *Journal of Environmental Chemical Engineering*, **11** (5), 110721, **2023**.
48. YIN Q., WANG Y., LI W., WEI C., CHEN Y., LIU C., LING X., CHEN Z. Highly efficient removal of contaminant from typical dye wastewater by using individual AOPs-A/O processes: Design, performance, and mechanism. *Journal of Environmental Chemical Engineering*, **12** (4), 113103, **2024**.
49. KORE V.S., MANJARE S.D., TARALKAR S.V. Intensified degradation of reactive blue 222 (RB222) textile dye by a hybrid AOP system of hydrodynamic cavitation coupled with inline UV and PMS oxidant. *Journal of Water Process Engineering*, **56**, 104472, **2023**.